Characterizations of Low-Frequency Zonal Flow in the Edge Plasma of the HL-2A Tokamak

A. D. Liu,[1] T. Lan,[1] C. X. Yu,[1] H. L. Zhao,[1] L. W. Yan,[2] W. Y. Hong,[2] J. Q. Dong,[2] K. J. Zhao,[2] J. Qian,[2] J. Cheng,[2] X. R. Duan,[2] and Y. Liu[2]

[1]*CAS Key Laboratory of Basic Plasma Physics, and Department of Modern Physics, University of Science and Technology of China, Hefei, Anhui 230026, China*

[2]*Southwestern Institute of Physics, P.O. Box 432, Chengdu, Sichuan 610041, China*

(Received 18 January 2009; published 27 August 2009)

A low-frequency (<4 kHz), poloidally and toroidally symmetrical potential structure that peaks near zero frequency is observed in the edge plasma of the HL-2A tokamak. The axisymmetry structure exhibits a radial coherence length less than 1 cm. These characteristics are consistent with the theoretically predicted low-frequency zonal flows (LFZF). The radial wave-number frequency spectra of the LFZF show that the LFZF packets propagate both outwards and inwards. The geodesic acoustic mode (GAM) is found to coexist with the LFZF, and the LFZF is found to modulate the GAM and ambient turbulence with in-phase and antiphase relations, respectively, through an envelope analysis.

DOI: 10.1103/PhysRevLett.103.095002 PACS numbers: 52.35.Ra, 52.25.Fi, 52.55.Fa

Self-organized structures [such as zonal flows (ZFs) [1])] arising from turbulence continue to be an active topic in magnetically confined fusion plasmas [2–4]. Zonal flows play a crucial role in regulating the level of turbulence and the associated transport. In toroidal plasmas, the ZFs are theoretically predicted to exist in two types: i.e., a stationary one with a near zero frequency, referred to as zero or low-frequency zonal flow (LFZF), and an oscillatory one with a higher frequency, called the geodesic acoustic mode (GAM). The experimental identification and characterization of zonal flows have been recently reported in a variety of toroidal fusion devices (see [5] for a review). It could be found that many results for the existence of the GAM have been provided while rather limited experimental evidence for the existence of the LFZF has only been obtained in the core region of toroidal plasmas. The toroidal and poloidal symmetry feature of the LFZF in core plasmas has been demonstrated, respectively, on the Compact Helical System (CHS) by the heavy ion beam probe [6] and on the Doublet III-D tokamak (DIII-D) by the beam emission spectroscopy [7,8]. In the edge region of toroidal plasmas, only some signatures of the LFZF presence have been observed using phase contrast imaging [9] and Langmuir probes [10–13]. However, no experimental evidence has previously been demonstrated for the coexistence of the LFZF and GAM in the edge region of toroidal plasmas, and no conclusive results of the three-dimensional spectral structure for the LFZF has been provided. In this Letter, we describe the first observation of the coexistence of the LFZF and GAM, and the three-dimensional spectral structure of the LFZF in the edge of a tokamak plasma. The interaction between the LFZF, GAM, and ambient turbulence (AT) is also analyzed.

Experiments were carried out on the HuanLiuqi-2A (HL-2A) in the limiter configuration with the major radius $R = 1.65$ m and minor radius $a = 0.40$ m. Discharges investigated were for Ohmically heated deuterium plasmas with the following parameters: plasma current $I_p = 160$–180 kA, toroidal magnetic field $B_\phi = 1.4$ T, and safety factor at the limiter position $q_a = 3.5$–4.0. Under such discharge conditions, MHD activity is very weak and does not interfere with the identification of LFZF and GAM. Measurements in the edge plasma were performed using two radially movable Langmuir probe systems, as shown in Fig. 1. The electron temperature, density, and their gradient scale lengths, as well as the ion-ion collisional frequency, are, respectively, $T_e = 30$–60 eV, $N_e = (0.2$–$0.5) \times 10^{13}$ cm^{-3}, $L_T = 4.5$–6.2 cm, $L_N = 2.4$–3.5 cm, and $\nu_{ii} = 4$–8 kHz at the measurement position $\rho = r/a \sim 0.9$. The first probe system consists of three arrays, one (marked as B) of which is located in the outer midplane and the others (marked as A and C) are located symmetrically about the outer midplane at

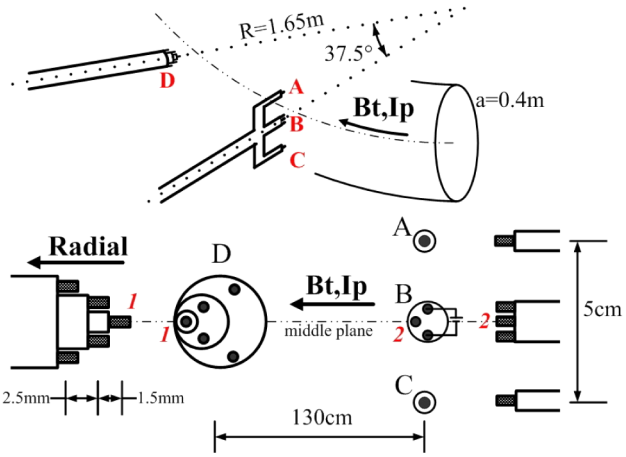

FIG. 1 (color online). The arrangement of experiments and the structures of probe arrays.

one cross section of the torus and poloidally separated by $d_\theta = 5.0$ cm. The second probe system is a three-step probe array (marked as D), located 130 cm toroidally away from the first system. Except for the probes in the array B, which were used as a triple probe for measuring the local electron temperature and density, all other probes were used to measure the floating potential. The three-step probes in the array D are used to detect changes in floating potentials within the radial range of a few millimeters. This arrangement of probes allows simultaneous measurements of floating potential fluctuations ($\tilde{\phi}_f$) in three dimensions with large poloidal and toroidal separations, thus enabling the determination of the spatial and temporal structures of ZFs. The sampling rate is 1 MHz, giving the Nyquist frequency of $f_N = 500$ kHz.

Figure 2(a) shows the power spectral densities of $\tilde{\phi}_f$, measured at $\rho \sim 0.9$, with different frequency resolutions, which are estimated as an ensemble average for a stationary interval of ~200 ms. Here the linear trend of every realization has been removed to eliminate the contamination induced by the effects of slow movement of bulk plasma or changes in plasma parameters. The spectra in the low-frequency range below 20 kHz exhibit two distinct spectral features: a coherent mode peaked at the frequency ~10 kHz and a low-frequency broadband (from zero extending up to 3 kHz) feature with the tendency of peaking near zero frequency as the frequency resolution gradually increases. Figures 2(b) and 2(c) provide the coherence and cross-phase spectra of potential fluctuations measured by probes located at the same flux surface with the separations of 5.0 cm poloidally and 130 cm toroidally. It can be seen that both features have high coherencies and phase shifts of zero. The poloidal and toroidal mode numbers are evaluated to be $m = 0.32 \pm 0.32$ and $n = 0.05 \pm 0.08$ for the low-frequency broadband feature and $m = 0.04 \pm 0.24$ and $n = 0.14 \pm 0.04$ for the coherent mode at ~9 kHz, respectively, all being much smaller than 1. The low-frequency broadband feature can be regarded as a poloidally and toroidally symmetric mode of $m = 0$ and $n = 0$, and is consistent with the theoretical prediction and simulation result [14,15] for the LFZF. The coherent mode at ~10 kHz has been identified to be the GAM observed previously [16,17], and will be analyzed further for comparison with the LFZF.

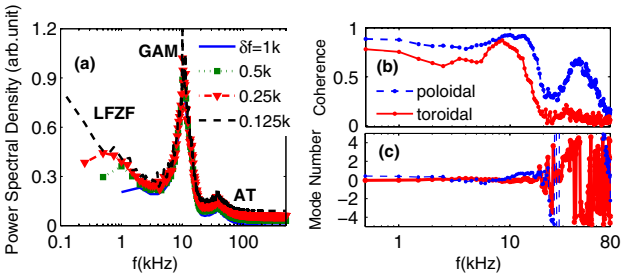

FIG. 2 (color online). (a) Power spectral density of $\tilde{\phi}_f$ under different frequency resolutions. (b) Coherence and (c) mode number spectra between two $\tilde{\phi}_f$ separated poloidally and toroidally. The frequency resolution is 0.5 kHz.

The radial spectral structure of the LFZF can be characterized with the local wave-number frequency spectrum $S(k_r, f)$ calculated using the two-point correlation technique [18]. Figures 3(a) and 3(b) provide the contour plot of the $S(k_r, f)$ spectrum for $\tilde{\phi}_f$ as well as the conditional spectrum $s(k_r|f) = S(k_r, f)/S(f)$, where $S(f) = \sum_{k_r} S(k_r, f)$, for the LFZF at the frequency 0.5 kHz and the GAM at the frequency 8.5 kHz. The wave-number resolution is chosen to be $\delta k = 1.06$ cm^{-1}, which is a trade off between reduction in the variance of the spectral estimate and loss of the wave-number resolution. It should be noticed that the radial correlation of potential fluctuations is measured by two probes (marked 1 and 2 as shown in Fig. 1) separated 1.5 mm radially and 130 cm toroidally to minimize the impact of the AT. A phase shift measured by the two probes is composed of both radial and toroidal components, i.e., $\Delta\theta_{12}(f) = k_r(f)d_r + k_\phi(f)d_\phi$. Because the toroidal phase shift for both the LFZF and GAM is zero as described above and its contribution is negligible, the cross phase $\Delta\theta_{12}(f)$ can be used to estimate the radial wave number $k_r(f)$ for the LFZF and GAM.

It can be seen from Figs. 3(a) and 3(b) that the spectra of $S(k_r, f)$ and $s(k_r|f)$ for the GAM are single-peaked, indicating that the GAM packet propagates radially outwards with little inward propagation component, according to the convention for the k_r sign adopted in this Letter. In contrast, the spectra for the LFZF appear to have two peaks at approximately symmetric positive and negative values $k_r \sim \pm 1.06$ cm^{-1} with a small imbalance in the positive and negative components. This is qualitatively similar to

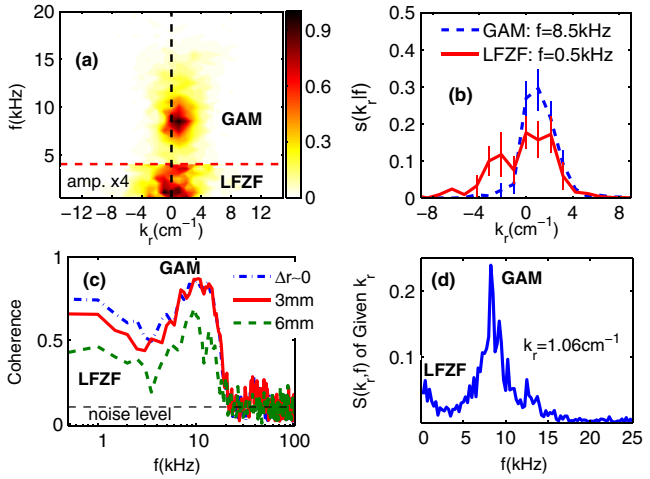

FIG. 3 (color online). (a) Normalized $S(k_r, f)$ below 20 kHz (the amplitude below the horizontal dashed line is multiplied by 4 for clarity). (b) $s(k_r|f)$ at $f = f_{\mathrm{GAM}}$ and $f = 0.5$ kHz. (c) Coherence spectra with different radial separations. (d) Power spectra for zonal flows at $k_r = 1.06$ cm^{-1}.

the simulation result [15] which shows that the frequency spectrum of LFZF is distributed over both positive and negative frequency ranges with peaks at about zero frequency. It should be pointed out that the model used in the simulation is the toroidal ion temperature gradient turbulence for core plasmas which may not apply to edge plasmas. This observation implies that the LFZF packet propagates in both the radially inward and outward directions with a net outward flow. These observations present a striking contrast to the characteristic radial structure of the GAM. The spectral averaged wave number and wave number width estimated from $s(k_r|f)$ are, respectively, $\bar{k}_r = 0.55\ \mathrm{cm}^{-1}$ and $\Delta k_r = 3.2\ \mathrm{cm}^{-1}$, which correspond to $\bar{k}_r\rho_i = 3.3 \times 10^{-2}$ and $\Delta(k_r\rho_i) = 0.19$. This is in the range for the LFZF expected by the simulation results of the drift Alfvén turbulence model for edge plasmas [19]. The radial structure of the LFZF can also be inferred from the radial dependence of the coherence spectra for $\tilde{\phi}_f$ measured by the probe tips 1 and 2 with increasing radial separation, as shown in Fig. 3(c). The spectra display that the coherence in the LFZF frequency range of 0–3 kHz decreases monotonically with increasing separation. This result allows us to estimate the radial correlation length of $0.5 < L_r^{\mathrm{LFZF}} < 1$ cm, which corresponds to approximately more than 10 times the ion cyclotron radius and is shorter than the correlation length of the GAM. This estimated correlation length is consistent with that observed on CHS [6] and DIII-D [7] devices, considering their overestimated values caused by the effect of the finite size of the sample volume for the heavy ion beam probe and beam emission spectroscopy measurements. This observation implies that the correlation length of the LFZF is much shorter than its mean wavelength and dominantly determines the shearing rate of the LFZF. Similar results have been obtained in the simulation [20], where it is found that the high k_r component of the LFZF can contribute significantly to the $E \times B$ shearing rate.

Figure 3(d) shows the power spectrum of ZFs at a given wave number of $k_r = 1.06\ \mathrm{cm}^{-1}$, deduced from $S(k_r, f)$. The spectral features for both the LFZF and GAM can be seen clearly from the figure: The LFZF spectrum has a peak at ~0.5 kHz with a width of ~1.5 kHz, corresponding to the correlation time of 0.7 ms which is much longer than that of AT (~10 μs). The GAM spectrum has a peak at 8.5 kHz with a width of ~3 kHz. This spectrum clearly shows that the LFZF intensity is much smaller than that of the GAM under our experimental conditions. This feature is consistent with the simulation results of drift Alfvén turbulence for edge plasmas [14] but in sharp contrast to the simulation [15] and observed results [6,7] in core plasmas, which reveal that the LFZF intensity is much larger than that of the GAM. This comparison is consistent with the theoretical prediction that the ZF intensity is dominated by the LFZF in the low q core region and the GAM in the high q edge region [21–23]. This may be the reason that the LFZF is more difficult to observe in the edge region.

In order to investigate the nonlinear interaction between the LFZF, the GAM, and the AT, the envelope analysis [24] is used. It is based on the analytic signal approach adopted in communication theory. The analytic signal is composed of a real signal and its Hilbert transform and the envelope is defined as the modulus of the analytic signal. The cross correlation between fluctuations and the envelope of fluctuations can be used to identify the nonlinear coupling between ZFs and AT. The coherence and cross-phase (divided by π) spectra between $\tilde{\phi}_{f_1}$ and the envelopes of filtered $\tilde{\phi}_{f_2}$ in the frequency ranges $f = 200$–500 kHz (referred to as the AT envelope) and $f = 7$–13 kHz (referred to as the GAM envelope), measured on the same flux surface, are shown in Figs. 4(a) and 4(b). The coherences clearly show that there are significant correlations between both the LFZF and GAM with the AT envelope but the coherence at the LFZF frequency is a factor of 3–4 smaller than that at the GAM frequency. The cross-phase spectra illustrate that the AT envelope delays both the LFZF and GAM by about π radians. These results indicate that the AT envelope is modulated by both the LFZF and the GAM with an antiphase relation and the smaller modulation amplitude induced by the LFZF is consistent with the smaller LFZF amplitude as compared with that of the

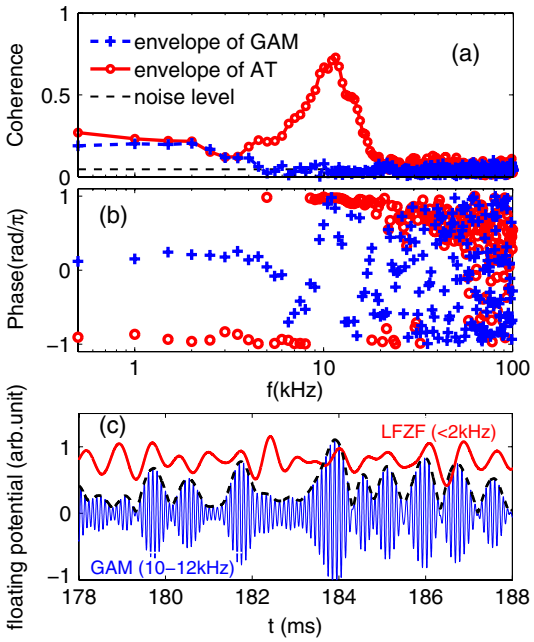

FIG. 4 (color online). (a) Coherence and (b) cross-phase spectra between $\tilde{\phi}_{f_1}$ and the envelope of filtered $\tilde{\phi}_{f_2}$ in the GAM frequency range (7–13 kHz) and the AT frequency range (200–500 kHz). (c) Time evolution of the GAM from $\tilde{\phi}_{f_2}$ and LFZF from $\tilde{\phi}_{f_1}$. The dash line is the envelope of GAM. ($\tilde{\phi}_{f_{1,2}}$ are the floating potential fluctuations on the same magnetic flux surface.)

GAM. It has been demonstrated previously in the analysis of the mechanism of the envelope modulation that the antiphase relation between the AT envelope and ZFs is dominantly caused by the amplitude modulation effect during the ZFs' generation [25]. Thus, this observation implies that both the LFZF and GAM gain or lose energy with the decrease or increase of the turbulence energy.

Moreover, the coherence and cross-phase spectra between $\tilde{\phi}_{f_1}$ and the GAM envelope of $\tilde{\phi}_{f_2}$ show that the GAM envelope is modulated by the LFZF with the in-phase relation, which is further supported by time evolutions of the GAM (10–12 kHz bandpass-filtered part of $\tilde{\phi}_{f_2}$) and the LFZF (0–2 kHz low-pass-filtered part of $\tilde{\phi}_{f_1}$) in Fig. 4(c). It can be generally seen that the intensity of the GAM is increased synchronously with the increasing of the LFZF intensity as irregular intermittent bursts. This is a conclusive evidence of the interaction between the LFZF and the GAM. This interaction was supposed to explain the so-called intermittency phenomena of the GAM observed in some experiments [26–28]. It should be mentioned that, although the intermittent dynamics of ZFs has been widely discussed theoretically [29–31], the interaction between the LFZF and the GAM is only reported in the simulation [14]. The possible explanation is that the LFZF and the GAM are correlated through the nonlinear interaction with the AT, which is the energy source for both the LFZF and the GAM. Briefly, all the results suggest that both the LFZF and the GAM are probably generated in the energy-conserving nonlinear interaction with the AT, as predicted by the theory [32,33].

In summary, the LFZF has been observed to be coexistent with the GAM in the edge plasma for the first time. The three-dimensional spectral features of the LFZF are identified to have many characteristics expected for the stationary zonal flow. In particular, the observation of the toroidal and poloidal symmetry provides the first conclusive evidence for the LFZF axisymmetry of theoretical predictions. The radial wave-number spectra exhibit that the LFZF packets radially propagate both outwards and inwards with a net outward flow. In addition, the AT envelope is modulated by both the LFZF and the GAM with the antiphase relation and the GAM envelope is found to be intermittently modulated by the LFZF with the in-phase relation, which imply that both the LFZF and the GAM are probably generated in the energy-conserving nonlinear interaction with AT, and the GAM intermittency is possibly caused by the interaction between LFZF and GAM. All the results demonstrate that the LFZF intensity is much smaller than that of the GAM in the higher q edge region, in agreement with expectations from theory and simulation.

The authors thank the HL-2A Team for support of these experiments, as well as Z. H. Lin and X. Q. Xu for the helpful comments. This work was supported by the Natural Science Foundation of China (Grants No. 10335060, No. 10875124, No. 10675041, No. 10775044), the Education Ministry of China (Grant No. 20060358059), and National Basic Research Program of China (Grant No. 2008CB717800).

[1] A. Hasegawa, C. G. Maclennan, and Y. Kodama, Phys. Fluids **22**, 2122 (1979).
[2] M. N. Rosenbluth and F. L. Hinton, Phys. Rev. Lett. **80**, 724 (1998).
[3] Z. Lin *et al.*, Science **281**, 1835 (1998).
[4] P. H. Diamond *et al.*, Plasma Phys. Controlled Fusion **47**, R35 (2005).
[5] A. Fujisawa *et al.*, Nucl. Fusion **47**, S718 (2007).
[6] A. Fujisawa *et al.*, Phys. Rev. Lett. **93**, 165002 (2004).
[7] D. K. Gupta, R. J. Fonck, G. R. Mckee, D. J. Schlossberg, and M. W. Shafer, Phys. Rev. Lett. **97**, 125002 (2006).
[8] G. R. Mckee *et al.*, in *Proceedings of the 21st IAEA Fusion Energy Conference, Chengdu, China, 2006* (IAEA, Vienna, 2007), No. EX/2-3.
[9] S. Coda, M. Porkolab, and K. H. Burrell, Phys. Rev. Lett. **86**, 4835 (2001).
[10] R. A. Moyer, G. R. Tynan, C. Holland, and M. J. Burin, Phys. Rev. Lett. **87**, 135001 (2001).
[11] G. S. Xu, B. N. Wan, M. Song, and J. Li, Phys. Rev. Lett. **91**, 125001 (2003).
[12] Y. Nagashima *et al.*, Phys. Rev. Lett. **95**, 095002 (2005).
[13] M. A. Pedrosa *et al.*, Phys. Rev. Lett. **100**, 215003 (2008).
[14] M. Ramisch, U. Stroth, S. Niedner, and B. Scott, New J. Phys. **5**, 12 (2003).
[15] T. S. Hahm *et al.*, Plasma Phys. Controlled Fusion **42**, A205 (2000).
[16] K. J. Zhao *et al.*, Phys. Rev. Lett. **96**, 255004 (2006).
[17] T. Lan *et al.*, Plasma Phys. Controlled Fusion **50**, 045002 (2008).
[18] J. M. Beall *et al.*, J. Appl. Phys. **53**, 3933 (1982).
[19] B. Scott, New J. Phys. **7**, 92 (2005).
[20] T. S. Hahm *et al.*, Phys. Plasmas **6**, 922 (1999).
[21] G. R. Mckee *et al.*, Phys. Plasmas **10**, 1712 (2003).
[22] K. Hallatschek, Plasma Phys. Controlled Fusion **49**, B137 (2007).
[23] B. Scott, Phys. Lett. A **320**, 53 (2003).
[24] D. Gabor, J. Inst. Electr. Eng. (London) **93**, 429 (1946).
[25] T. Lan *et al.*, Phys. Plasmas **15**, 056105 (2008).
[26] G. D. Conway *et al.*, Plasma Phys. Controlled Fusion **47**, 1165 (2005).
[27] A. V. Melnikov *et al.*, Plasma Phys. Controlled Fusion **48**, S87 (2006).
[28] A. Fujisawa *et al.*, Plasma Phys. Controlled Fusion **49**, 211 (2007).
[29] Z. Lin *et al.*, Phys. Rev. Lett. **83**, 3645 (1999).
[30] M. A. Malkov, P. H. Diamond, and M. N. Rosenbluth, Phys. Plasmas **8**, 5073 (2001).
[31] K. Miki, Y. Kishimoto, N. Miyato, and J. Q. Li, Phys. Rev. Lett. **99**, 145003 (2007).
[32] L. Chen, Z. Lin, and R. B. White, Phys. Plasmas **7**, 3129 (2000).
[33] P. H. Diamond *et al.*, Nucl. Fusion **41**, 1067 (2001).